Supporting Information

Signature of pressure-induced topological phase transition in non-centrosymmetric elemental Tellurium

T. Ideue[a], M. Hirayama[b], H. Taiko[a], T. Takahashi[c], M. Murase[c],

T. Miyake[d], S. Murakami[e,f], T. Sasagawa[c], and Y. Iwasa[a,b]

1. **Fermi level position for each sample**
2. **Sample information**
3. **Detailed behavior of the pressure-induced band evolution**
4. **Pressure variation of δ in sample 1 and 2**
5. **ρ_{zz} oscillations v.s. σ_{zz} oscillations in sample 1 and 2**
6. **SdH oscillations in sample 3 and 4**
7. **SdH oscillations in sample 5 and 6 ($\boldsymbol{B} \parallel \boldsymbol{I} \parallel \boldsymbol{z}$)**

www.pnas.org/cgi/doi/10.1073/pnas.1905524116

1. Fermi level position for each sample

We discuss the Fermi level position of each sample by comparing the calculated cross-sectional area of Fermi surface at ambient pressure with those obtained in the experiment. Figure S1 shows the band structure at ambient pressure obtained by the first principle calculation. Energy level of the minimum of the camel-back-like valence band dispersion (E_c) at H point is around E = -2 meV measured from the valence band top. Shape of the calculated there-dimensional Fermi surface at E_F = -2 meV actually shows the critical behavior (nearly connected two Fermi surfaces, Fig. S1B). Calculated cross-sectional area of the Fermi surface at E_F = 2 meV (S_F = 0.592× 10^{-3} $Å^{-2}$) is larger than that of sample 1, while double of it is smaller than those of sample 2, 3, and 4. Thus, we can conclude that Fermi level of sample 1 locates above E_c while those of sample 2, 3, and 4 are below E_c.

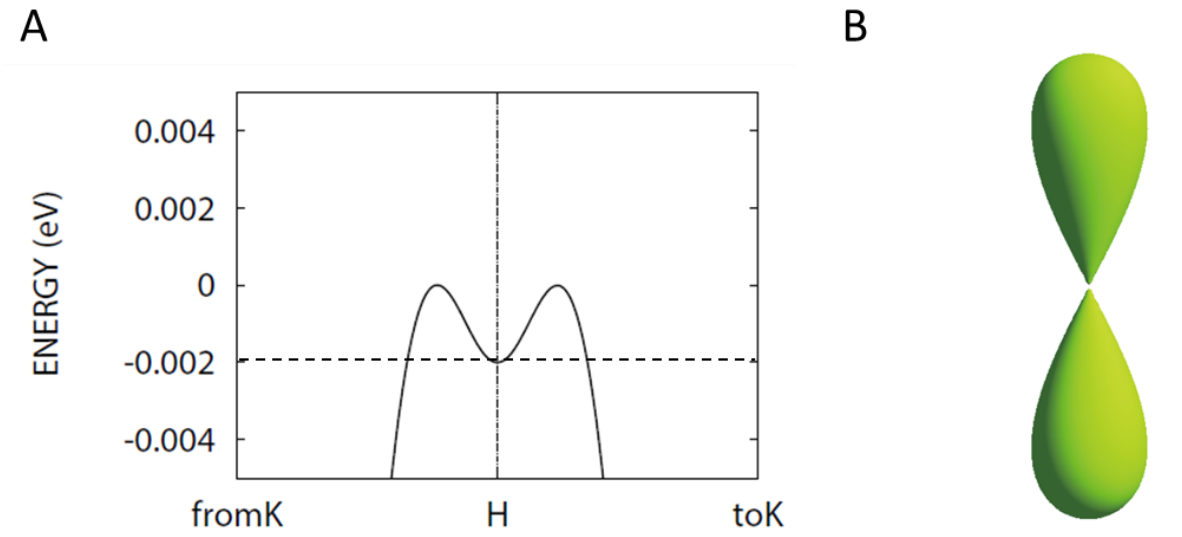

Fig. S1. Fermi surface around E_c = -2 meV. (*A*) First principle calculation of Te band at ambient pressure. Minimum of the camel-back-like valence band dispersion (E_c) locates around E_c = -2 meV. (*B*) Calculated there-dimensional Fermi surface for E_F = -2 meV.

2. Sample information

In Table S1, we show the carrier density n_{Hall} estimated from Hall effect, mobilityμ (P = 0 GPa) and μ (P = 3 GPa) at T = 2 K, cross-sectional area of the Fermi surface S_{F} calculated from period of SdH oscillations, and corresponding Fermi wave number k_{F} or effective carrier density n_{eff} under ambient pressure for each sample. In the calculation of k_{F} or n_{eff}, we assumed the simple isotropic linear band dispersion and several relations between parameters (based on the discussion in Nat. Mater. **14** 280 (2015)). We note that such an assumption is no longer valid in this system with large anisotropy and rather complex band structure. Nevertheless, n_{Hall} and n_{eff} show consistent values. From the temperature variation of SdH oscillations in sample 2 (Fig.4), we obtained the Fermi velocity v_{F} = 4.0× 10^{4} m/s and quantum lifetime τ_{Q} = 1.4 × 10^{-13} s of ample 2 at P = 3 GPa. Transport lifetime defined by $\tau_{\mathrm{transport}} = \mu\hbar k_{\mathrm{F}}/ev_{\mathrm{F}}$ is estimated as $\tau_{\mathrm{transport}} = 8.5 \times 10^{-12}$ s, which is order of magnitude larger than τ_{Q}. ($\tau_{\mathrm{transport}}$ generally larger than τ_{Q}, since $\tau_{\mathrm{transport}}$ measures backscattering process that relaz the current while τ_{Q} is sensitive to all processes that cause Landau level broadening.

We also show the calculated carrier density n_{cal} and S_{F} at E_{F} = −1, −3, and −5 meV in Table S2. Experimentally obtained values of n and S_{F} in Table S1 show the similar values at E_{F} = −1 meV for sample 1 and E_{F} = −5 meV for sample 2~4, respectively (Fig. S2). Thus, we discuss the qualitative behavior of the pressure-induced topological phase transition by using the calculated values for E_{F} = −1 meV (sample 1, Fig. 2F) and E_{F} = −5 meV (sample 2, Fig. 3F).

Sample	n_{Hall} (cm^{-3})	μ (cm^2/Vs) (P = 0 GPa)	μ (cm^2/Vs) (P = 3 GPa)	S_F (10^{-3} Å^{-2})	k_F (Å^{-1})	n_{eff} (cm^{-3})
1	2.7×10^{16}	6400	33000	0.5	0.0126	6.7×10^{16}
2	4.13×10^{17}	3100	31000	1.87	0.0244	4.9×10^{17}
3	2.0×10^{17}	1000	—	—	—	—
4	6.25×10^{17}	1000	—	1.76	0.0237	4.5×10^{17}

Table S1. Carrier density n_{Hall} estimated from Hall effect, mobilityμ (P = 0 GPa) and μ (P = 3 GPa) at T = 2 K, cross-sectional area of the Fermi surface S_F calculated from period of SdH oscillations, and corresponding Fermi wave number k_F or effective carrier density n_{eff} under ambient pressure for each sample.

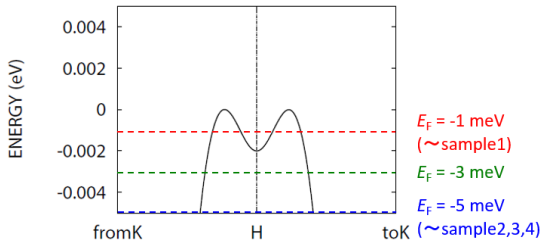

E_F (meV)	n_{cal} (cm^{-3})	$S_{F\,cal}$ (10^{-3} Å^{-2})
-1	1.4×10^{16}	0.12
-3	0.8×10^{17}	0.88
-5	1.8×10^{17}	1.4

Fig. S2. (left) Schematics of Fermi level (E_F = −1, −3, and −5 meV.).

Table S2. (right) Calculated carrier density n_{cal} and S_F at E_F = −1, −3, and −5 meV.

3. Detailed behavior of the pressure-induced band evolution

In Figs. S3 A-L, we show the detailed pressure-induced band evolution.

In Figs. A, C, E, G, I, K we show both conduction and valence bands. Figs. B, D, F, H, J, L are the magnified view of valence band.) We calculate all band structures by the fully-relativistic Hamiltonian with the GW self-energy correction.

Conduction band continuously decreases by applying the pressure and finally touches around P = 2 GPa. As shown in Figs. S3 B and D, Fermi level of sample 1 (E_F~−1meV) will cross the minimum of the camel-back-like valence band dispersion between P = 0 GPa and P = 0.6

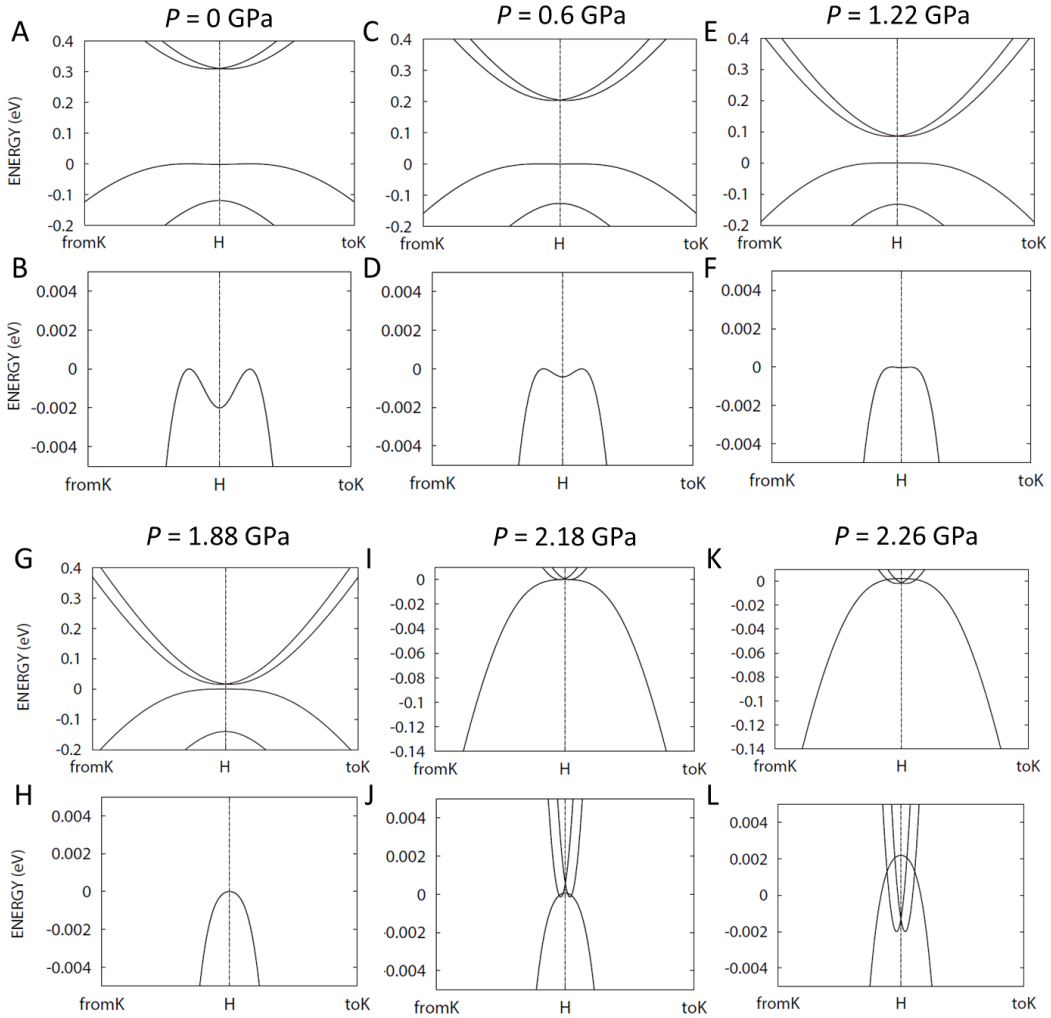

GPa, leading to Lifshitz transition in this sample.

Fig. S3. Pressure-induced band evolution of Te. P = 0 GPa (A and B), 0.6 GPa (C and D), 1.22 GPa (E and F), 1.88 GPa (G and H), 2.18 GPa (I and J), and 2.26 GPa (K and L).

4. Pressure variation of δ in sample 1 and 2

In addition to the period of oscillations, which provides us with information of the cross-sectional area of Fermi surface, the phase of SdH oscillations (or intercept of the index plot) also offers the important insight into the band dispersion or Berry phase originating from spin texture. Figures S4 A (C) and B (D) show the magnified view of the index plot and pressure dependence of δ of sample 1 (sample 2). δ shows crossover behavior from -0.2 in the semiconducting phase to 0.1 in the Weyl semimetal phase, possibly reflecting the change of band dispersion. However, the value of δ are not 0 (parabolic dispersion) nor 1/2 (Dirac dispersion), varying from -0.2 to 0.1, potentially due to the complex spin texture/dispersion of valence band in Te. It is also noted that analysis of the phase of SdH oscillations δ in topological semimetal is not simple as discussed in Nat. Mater. **14** 280 (2015) or Science **350** 413 (2015). Quantitative argument of δ and its relation to the complex spin texture should be further studied in the future.

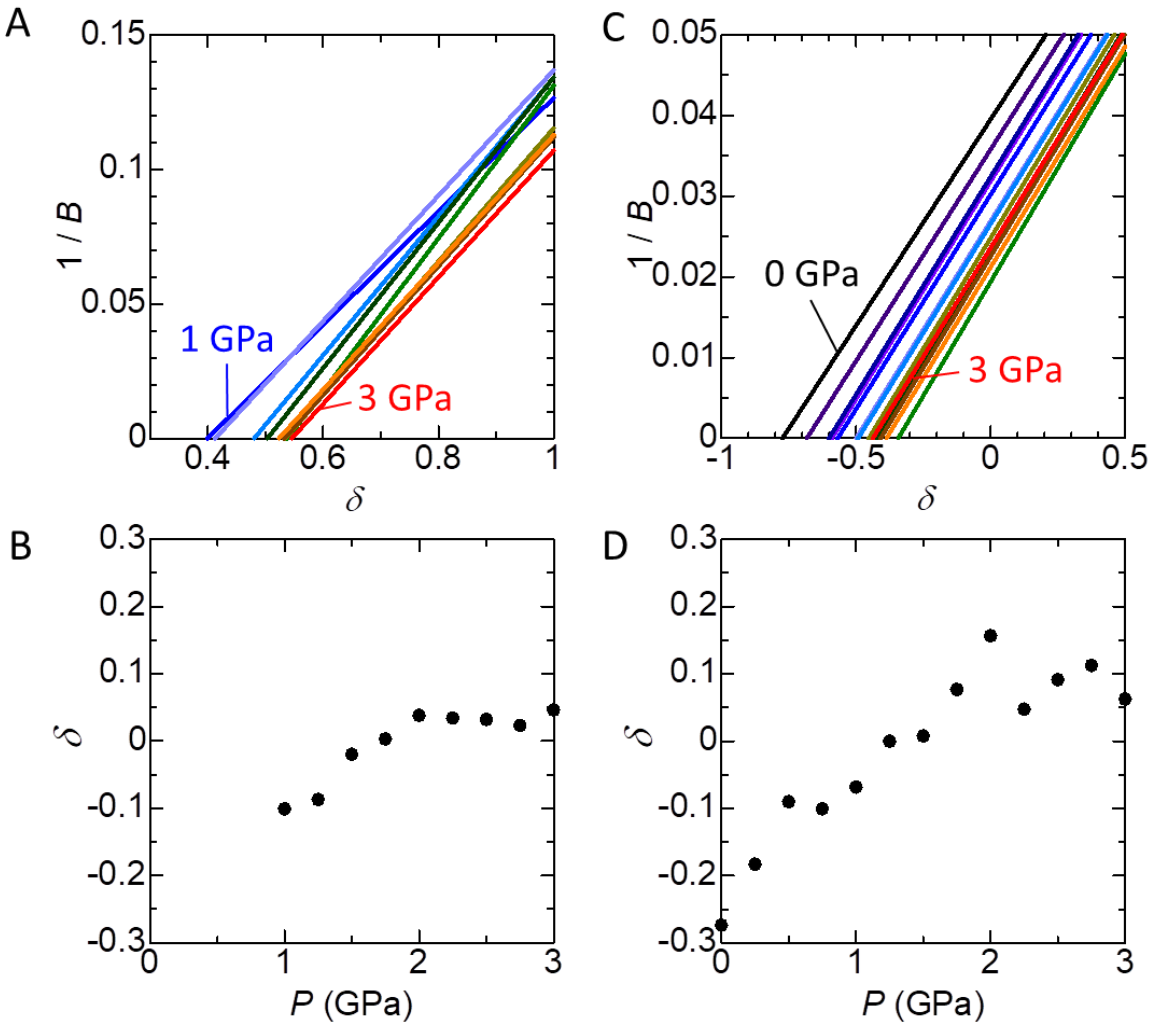

Fig. S4. Pressure variation of δ in sample 1 and 2. (*A*, *B*) Magnified view of the index plot (A) and pressure dependence of δ (B) of sample 1. (*C*, D) Magnified view of the index plot (C) and pressure dependence of δ (D) of sample 2.

5. ρ_{zz} oscillations v.s. σ_{zz} oscillations in sample 1 and 2

In the main text, we argue the ρ_{zz} oscillations of sample 1 and sample 2. In this section, we compare σ_{zz} oscillations with those in ρ_{zz}. In Figs. S5 and Figs. S6, we show the oscillating components of σ_{zz} (A), index plots (B), and pressure variation of the horizontal axis intercept δ in index plots (C) of sample 1 (Figs. S5) and sample 2 (Figs. S6), respectively. Since Hall angle is large enough in both samples, oscillating components in σ_{zz} show similar behavior as those in ρ_{zz}; i.e., $\Delta\sigma_{zz}\sim\Delta\rho_{zz}$. Following the index plots of $\Delta\rho_{zz}$ in the main text, we assigned minimum of $\Delta\sigma_{zz}$ as an integer in Fig. S5B and Fig. S6B δ shows crossover behavior from semiconducting phase to Weyl semimetal phase, which is almost consistent with that of ρ_{zz} oscillations.

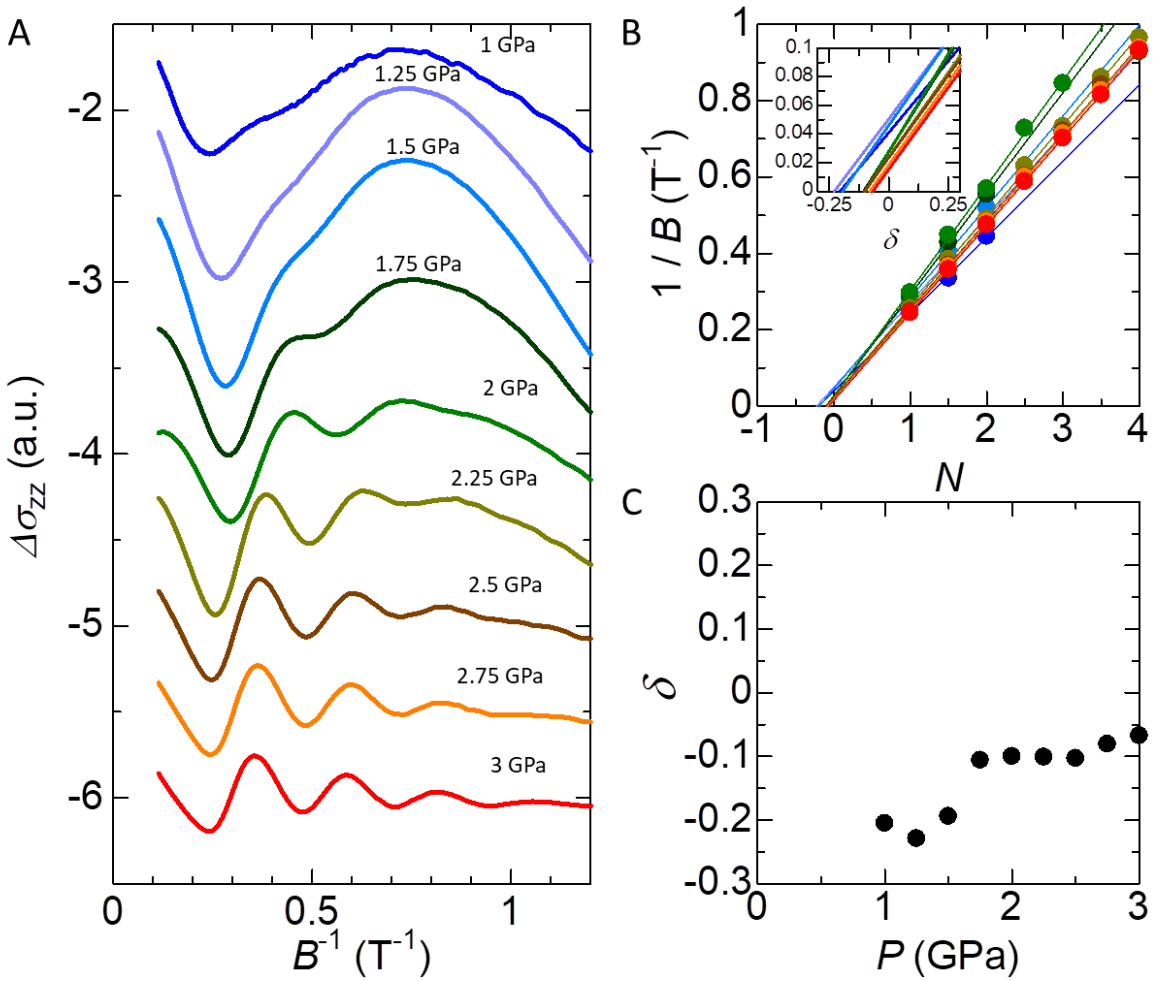

Fig. S5. σ_{zz} oscillations of sample 1. (*A*) SdH oscillations of σ_{zz} in sample 1. (*B*) Index plot for σ_{zz} oscillations in sample 1. (*C*) Pressure variation of the horizontal axis intercept δ in the index plot. δ shows the similar crossover behavior toward P = 2 GPa as that for ρ_{zz} oscillations.

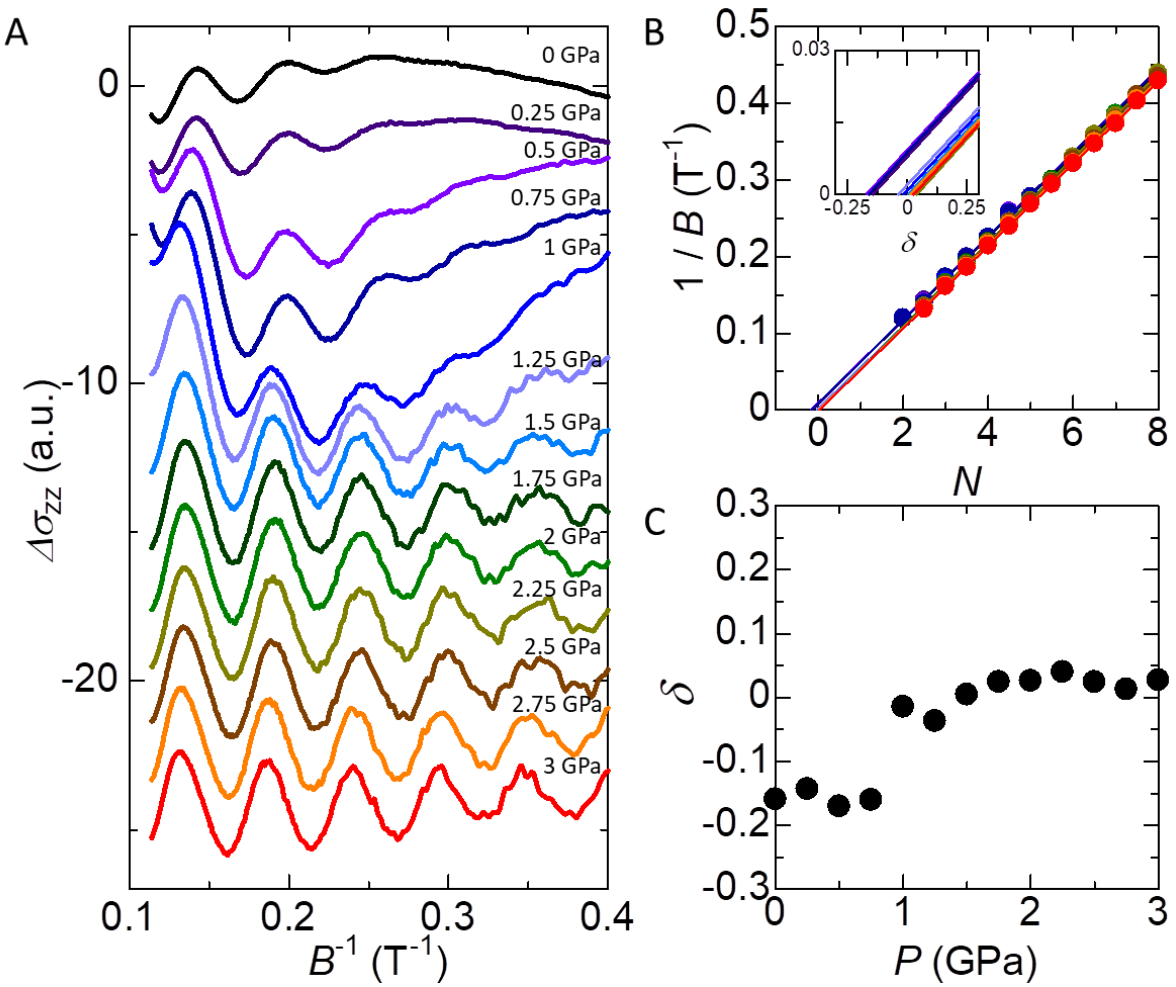

Fig. S6. σ_{zz} oscillations of sample 2. (*A*) SdH oscillations of σ_{zz} in sample 2. (*B*) Index plot for σ_{zz} oscillations in sample 2. (*C*) Pressure variation of the horizontal axis intercept δ in the index plot. δ shows the similar crossover behavior toward P = 2 GPa as that for ρ_{zz} oscillations.

6. SdH oscillations in sample 3 and 4

Anomaly of the Fermi surface cross-sectional area S_F has been also observed in sample 3 and sample 4. In Fig. S7, we show the oscillating components of sample 3 (Fig. S7 A) and sample 4 (Fig. S7 B) under various pressures. S_F calculated from the period of oscillation as a function of pressure are displayed in Fig. S7 C (sample 3) and Fig. S7 D (sample 4), respectively. According to the oscillation periods, the Fermi levels of both samples are estimated to locate below E_c (See above section 1). Therefore, pressure-induced Lifshitz transition which has been observed in sample 1 cannot be expected for both samples similarly to sample 2. Importantly, however, S_F of both samples still shows anomaly around P = 2 GPa, which almost coincides with the theoretically predicted pressure for the topological phase transition; it shows the decreasing behavior toward P = 2 GPa and increases afterwards. These results indicate that measurement of SdH oscillations is a powerful probe for topological phase transition in Te even if Fermi level is slightly away from the valence band maximum.

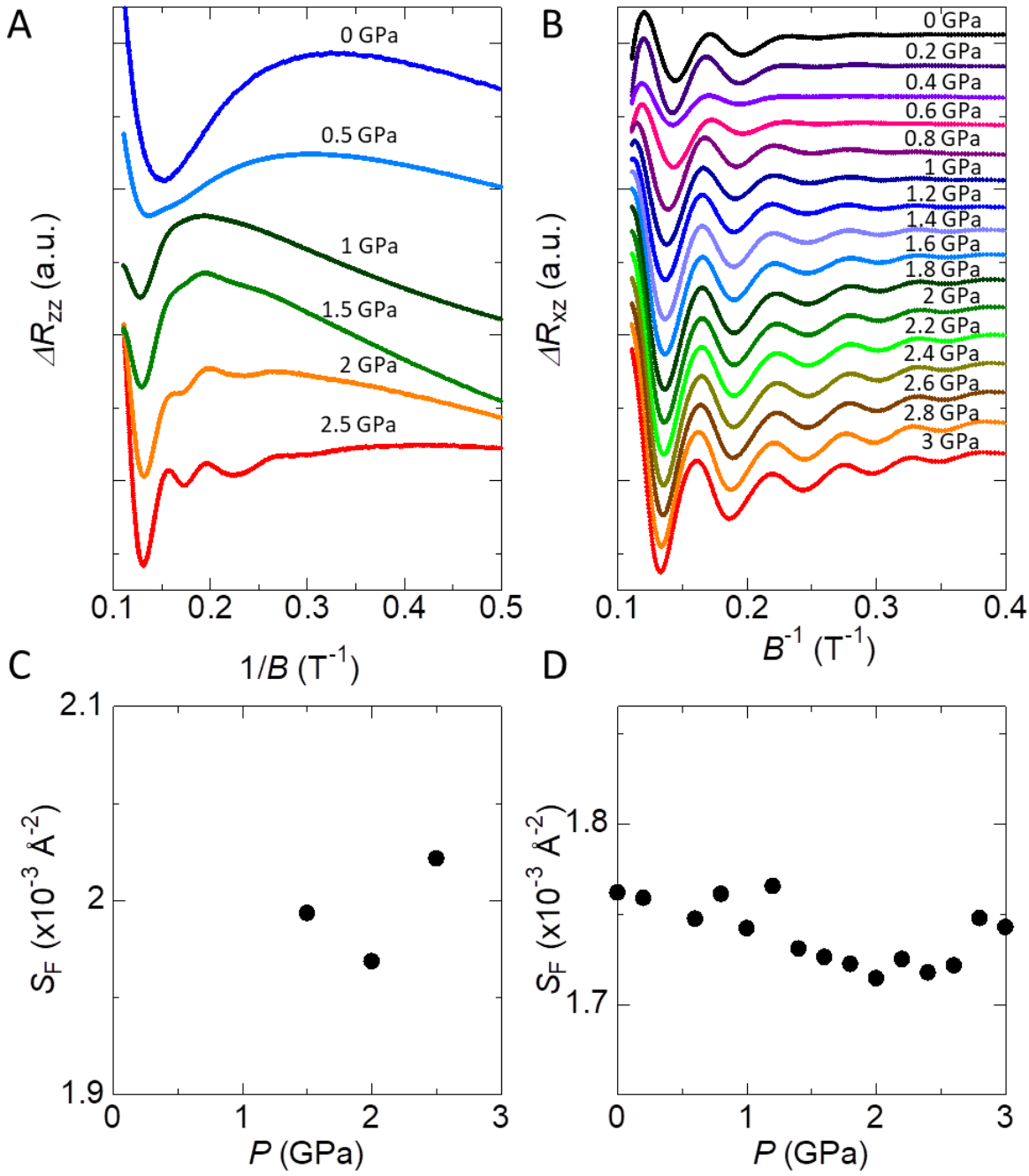

Fig. S7. SdH oscillations in sample 3 and 4. (*A* and *B*) SdH oscillations of sample 3 (A) and sample 4 (B). (*C* and *D*) Pressure dependence of the cross-sectional area of Fermi surface (S_F) estimated from the periods of oscillations. S_F of both sample 3 (C) and sample 4 (D) show similar anomaly around P = 2 GPa as that of sample 2 in the main text.

7. SdH oscillations in sample 5 and 6 ($\boldsymbol{B \parallel I \parallel z}$)

We further studied pressure dependence of SdH oscillations of Te in another configuration ($B \parallel I \parallel z$).

Figs S8 and S9 show the magnetoresistance (A), oscillating components of the resistance (B), index plots (C), and pressure dependence of the cross-sectional area of Fermi surface (D) for sample 5 (Fig. S8) and sample 6 (Fig. S9), respectively. In these samples, we applied both current and magnetic field parallel to the *z* axis. Judging from the values of S_F, Fermi level of sample 5 and 6 are considered to locate below E_c. ($S_F = 0.16 \times 10^{-3}$ Å^{-2} when $E_F = E_c = -2$ meV, which is smaller than those of sample 5 and 6.) In this configuration, periods of SdH oscillations reflects the maximal cross section of dumbbell-shaped Fermi surface which is illustrated by solid line in Fig. S10. This area is not sensitive to the topological phase transition which mainly affects the neck position drawn by dashed line in Fig. S10. Actually, anomaly of S_F around P = 2 GPa is small and hard to see (Figs. S8 D and S9 D). Instead, S_F of both samples show the clear upturn around P = 0.6 GPa, which coincides with the pressure at which camel-back-like valence band dispersion disappears. It is considered that disappearance of the camel-back-like valence band dispersion can be more sensitively probed in this configuration than the configuration discussed in the main text ($B \perp I \parallel z$).

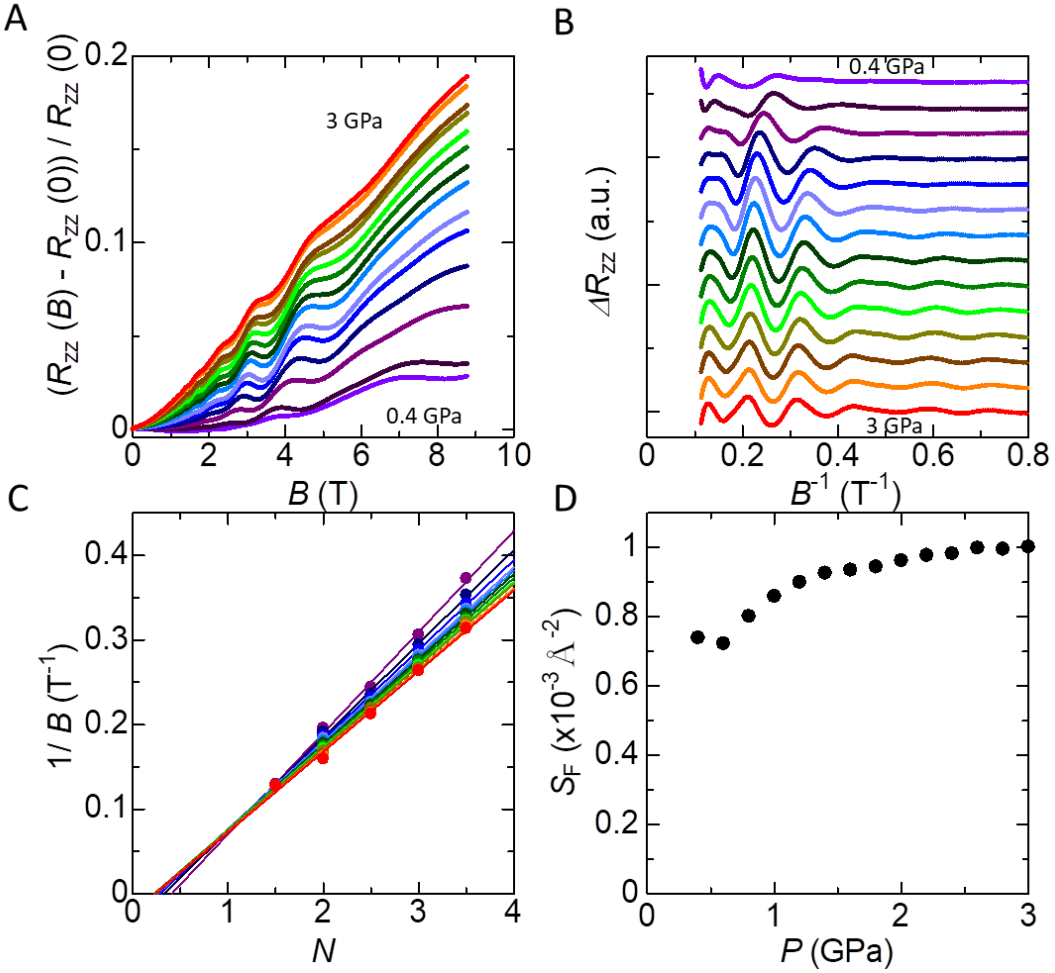

Fig. S8. SdH oscillations of sample 5 ($B \parallel I \parallel z$). (*A* and *B*) Magnetoresistance (A) and oscillating components (B) of the resistance calculated by subtracting the polynomial background from A. (*C*) Index plots for each pressure. (*D*) Pressure dependence of the cross-sectional area of Fermi surface estimated from the periods of oscillations.

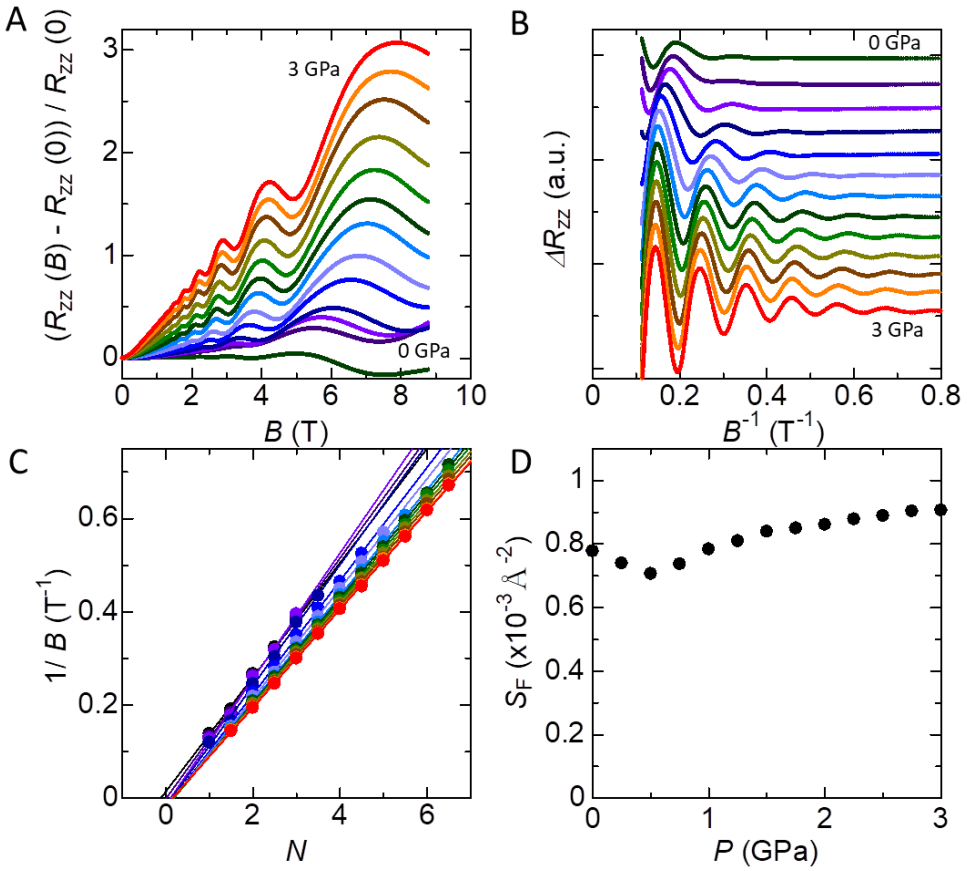

Fig. S9. SdH oscillations of sample 6 ($B \parallel I \parallel z$). (*A* and *B*) Magnetoresistance (A) and oscillating components (B) of the resistance calculated by subtracting the polynomial background from A. (*C*) Index plots for each pressure. (*D*) Pressure dependence of the cross-sectional area of Fermi surface estimated from the periods of oscillations.

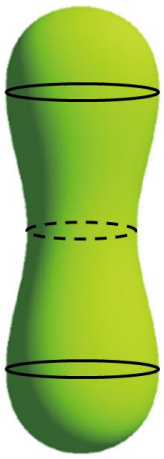

Fig. S10. Fermi surface and maximal (solid lines)/ minimal (dashed line) cross sections.